Article

A stable zeolite with atomically ordered and interconnected mesopore channel

https://doi.org/10.1038/s41586-024-08206-1

Received: 8 January 2024

Accepted: 11 October 2024

Published online: 11 December 2024

Open access

Check for updates

Peng Lu[1,5]✉, Jiaoyan Xu[2,5], Yiqing Sun[1,5], Rémy Guillet-Nicolas[3], Tom Willhammar[2], Mohammad Fahda[3], Eddy Dib[3], Bo Wang[4], Zhengxing Qin[4], Hongyi Xu[2], Jung Cho[2], Zhaopeng Liu[1], Haijun Yu[1], Xiaobo Yang[1], Qiaolin Lang[1], Svetlana Mintova[3], Xiaodong Zou[2] & Valentin Valtchev[3]✉

Zeolites are crystalline microporous materials constructed by corner-sharing tetrahedra (SiO_4 and AlO_4), with many industrial applications as ion exchangers, adsorbents and heterogeneous catalysts[1–4]. However, the presence of micropores impedes the use of zeolites in areas dealing with bulky substrates. Introducing extrinsic mesopores, that is, intercrystal/intracrystal mesopores, in zeolites is a solution to overcome the diffusion barrier[5–8]. Still, those extrinsic mesopores are generally disordered and non-uniform; moreover, acidity and crystallinity are always, to some extent, impaired[9]. Thus, synthesizing thermally stable zeolites with intrinsic mesopores that are of uniform size and crystallographically connected with micropores, denoted here as intrinsic mesoporous zeolite, is highly desired but still not achieved. Here we report ZMQ-1 (Zeolitic Materials, Qingdao Institute of Bioenergy and Bioprocess Technology, no. 1), an aluminosilicate zeolite with an intersecting intrinsic meso-microporous channel system delimited by 28 × 10 × 10-rings, in which the 28-ring has a free diameter of 22.76 Å × 11.83 Å, which reaches the mesopore domain. ZMQ-1 has high thermal and hydrothermal stability with tunable framework Si/Al molar ratios. ZMQ-1 is the first aluminosilicate zeolite with an intrinsic meso-microporous channel system. The Brønsted acidity of ZMQ-1 imparts high activity and unique selectivity in the catalytic cracking of heavy oil. The position of the organic structure-directing agent (OSDA) used for ZMQ-1 synthesis was determined from three-dimensional electron diffraction (3D ED) data, which shows the unique structure-directing role of the OSDA in the formation of the intrinsic meso-microporous zeolite. This provides an incentive for preparing other stable mesopore-containing zeolites.

The quest for synthesizing mesoporous zeolites with pores larger than 20 Å (refs. 10,11) has persisted for decades, as the large-pore industrially relevant zeolites exhibit pore openings of less than 7.5 Å (refs. 12–14). Several aluminosilicate molecular sieves with intrinsic mesopores of size in the range 20–300 Å, such as M41S family materials[15,16], were reported, but they demonstrated relatively low thermal/hydrothermal stability and weak acidity owing to their amorphous nature[17]. So far, there are only two reported meso-microporous germanosilicate zeolites with pore openings that reached the mesopore range, that is, ITQ-37 (**-ITV**) (30-ring, 19.3 × 4.3 Å)[18] and ITQ-43 (**-IRT**) (28-ring, 21.2 × 4.1 Å)[19] (Supplementary Table 1). Unfortunately, those zeolites are not stable after the removal of OSDAs, thus hindering their practical application. Recently, stable aluminosilicate and pure-silicate zeolites with extra-large pores (pores delimited by rings greater than 12 tetrahedral atoms) of 16MR (10.6 Å, **JZO**)[20], 16MR (10.36 Å, **JZT**)[21] and 20MR (14.3 Å, ZEO-5)[22] were realized by using a phosphorus-containing bulky OSDA, pushing the channel size towards the mesopore region. However, the synthesis of stable aluminosilicate zeolites with intrinsic mesopores has not yet been achieved. Here we demonstrate that ZMQ-1 is the first attainment, to our knowledge, of such a goal reaching a 28-ring pore with a free diameter of 22.76 Å.

Synthesis of ZMQ-1 zeolite

ZMQ-1 was synthesized using a bolaform phosphonium-based OSDA (denoted as Tri-Cy-dC8; see Extended Data Fig. 1a and Supplementary Figs. 1 and 2) through conventional hydrothermal crystallization (see Methods for detailed synthesis procedures). Comparing ammonium-based OSDAs massively used in zeolite synthesis and phosphonium-based ones, the latter offer a stronger positive charge and flexibility of cyclohexyl groups, an advantage in the quest for extra-large-pore zeolites. Furthermore, the phosphonium-based OSDAs

[1]The ZeoMat Group, Key Laboratory of Photoelectric Conversion and Utilization of Solar Energy, Qingdao New Energy Shandong Laboratory, Qingdao Institute of Bioenergy and Bioprocess Technology, Chinese Academy of Sciences, Qingdao, China. [2]Department of Materials and Environmental Chemistry, Stockholm University, Stockholm, Sweden. [3]Laboratoire Catalyse et Spectrochimie, Normandie University, ENSICAEN, UNICAEN, CNRS, Caen, France. [4]State Key Laboratory of Heavy Oil Processing, College of Chemistry and Chemical Engineering, China University of Petroleum (East China), Qingdao, China. [5]These authors contributed equally: Peng Lu, Jiaoyan Xu, Yiqing Sun. ✉e-mail: lupeng@qibebt.ac.cn; valentin.valtchev@ensicaen.fr

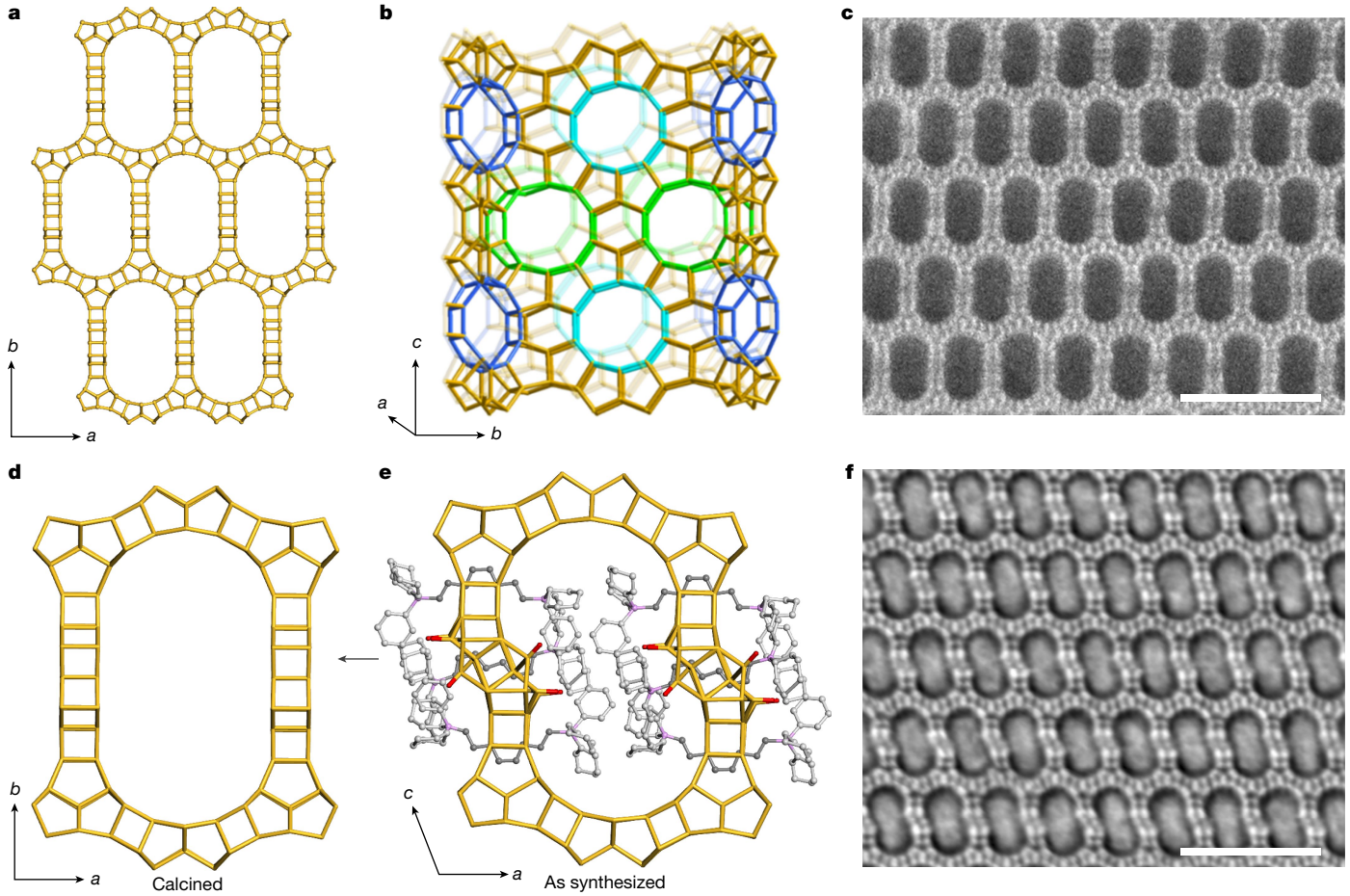

Fig. 1 | The structures and STEM images of calcined and as-synthesized ZMQ-1. a–**d**, Calcined ZMQ-1. **a**, The structure viewed along the *c* axis shows the 28-ring channels. **b**, A 28-ring channel viewed approximately along the *a* axis shows the 10-ring windows that connect adjacent 28-ring channels. There are six respective four 10-rings at the same height, which alternate along the *c* axis. The colours represent three symmetry-independent 10-ring windows. **c**, ADF-STEM image acquired along the *c* axis showing the extra-large 28-ring channels. **e**,**f**, As-synthesized ZMQ-1. The extra-large 28-ring channel shows the locations of OSDAs determined from low-dose cryo-cRED data. The bilobal-shaped 28-ring channel (**e**) is transformed into an elliptical-shaped 28-ring channel (**d**) following calcination and the removal of the OSDAs. The terminal hydroxyl groups condense to form a fully four-connected framework. Colour code: red, terminal oxygen; purple, phosphorus; dark grey, carbon determined by 3D ED data; light grey, carbon not located by 3D ED and added based on chemical information (they are not included in the experimental cif file). Only the T···T connections of the framework are shown and H atoms are omitted for clarity. **f**, iDPC-STEM image of the as-synthesized ZMQ-1 taken along the 28-ring channels showing the bilobal-shaped pores. Scale bars, 5 nm.

exhibit higher hydrothermal stability and can be used under harsher hydrothermal conditions. Our focus on a bolaform phosphonium-based OSDA with a relatively long methylene chain between the positively charged bulky and rigid heads is justified by the fact that the latter feature could generate a large pore space, whereas the long distance between the charged heads leaves enough space for the formation of zeolite framework.

ZMQ-1 was first discovered in a hydroxide medium at a synthesis temperature of 180 °C and the crystallization was accelerated at 190 °C (Extended Data Fig. 2a). Despite the high synthesis temperature, the OSDA was found to be intact in the as-synthesized zeolites (Extended Data Fig. 1b,c). The Si/Al molar ratio of ZMQ-1 zeolite could be tuned in a wide range from about 15 to 70 (Extended Data Fig. 2b), which endows it with versatilities for applications that require different acidic properties. Besides, we successfully obtained ZMQ-1 zeolites using different Si and Al sources and various compositions (Extended Data Fig. 2c), proving the robustness of the synthesis. It took longer crystallization time to obtain ZMQ-1 zeolite in a fluoride medium (Extended Data Fig. 2d). The morphology of ZMQ-1 obtained in hydroxide and fluoride media is individual and aggregated rectangular prisms, respectively, with the maximum size of about 2 μm (Extended Data Fig. 3). The synthesis compositions, crystallization conditions and phases obtained are summarized in Supplementary Table 2.

Structure determination of ZMQ-1

The size of ZMQ-1 crystals was too small for single-crystal X-ray diffraction. Its structure was determined by 3D ED, more specifically, continuous rotation electron diffraction (cRED)[23] (Fig. 1 and Extended Data Fig. 4). cRED data show that the calcined ZMQ-1 is orthorhombic and the unit-cell parameters were further refined against the powder X-ray diffraction (PXRD) data by Pawley fitting to be a = 18.83(10) Å, b = 54.9(2) Å and c = 20.36(5) Å (Supplementary Table 3 and Extended Data Fig. 5a). The space group *Cmmm* (no. 65) was used for the structure determination, based on the observed reflection conditions (Extended Data Fig. 4a–c). The structure of the calcined ZMQ-1 has a 3D 28 × 10 × 10-ring channel system with the extra-large pore delimited by 28 T-atoms (Fig. 1 and Supplementary Video 1). The 28-ring channels are interconnected by 10-rings (Fig. 1b). There are three symmetry-independent 10-ring windows; each contains two rings and connects two adjacent 28-ring channels. Two windows are perpendicular to the *a* axis: one built by double 10-rings (#1, in cyan) and one by 10-rings and 12-rings

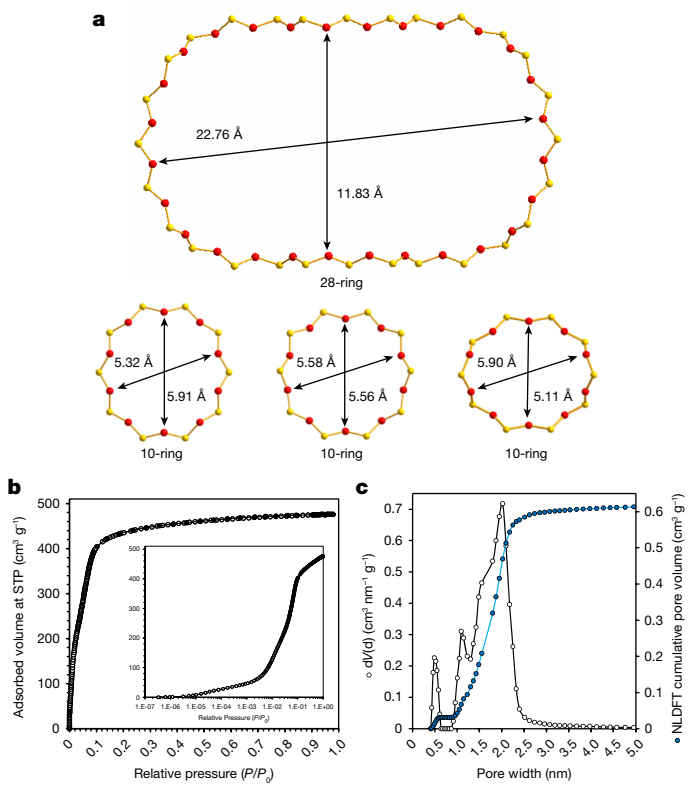

Fig. 2 | Porosity analysis of ZMQ-1. a, Free diameters of the 28-ring and 10-rings in calcined ZMQ-1, in which the diameter of oxygen (2.70 Å) has been subtracted. **b**, Ar 87 K adsorption–desorption isotherm of the ZMQ-1 zeolite (semilogarithmic scale in inset). **c**, Corresponding cumulative pore volume plot and pore size distribution calculated using a dedicated NLDFT metastable adsorption branch kernel (assuming Ar adsorption in cylindrical zeolitic pores). STP, standard temperature and pressure.

(#2, in green). The third one is perpendicular to the [±510] directions, built from two 10-rings (#3, in blue). Four 10/12-ring windows (#2) are located at $z = 0$ and six 10/10-ring windows at $z = ½$ in sequence #133133. To our knowledge, ZMQ-1 is the first stable aluminosilicate zeolite containing 28-ring channels. It has a fully tetrahedrally connected zeolite structure instead of the 'interrupted framework' featured by other extra-large-pore zeolites (EMM-23 (**-EWT**), NUD-6 and SSZ-70)[24–26]. The free pore diameters are 22.76 Å × 11.83 Å for the 28-ring channel and 5.91 Å × 5.32 Å (#1), 5.56 Å × 5.58 Å (#2) and 5.11 Å × 5.90 Å (#3) for the 10-ring windows (Fig. 2a). Thus, ZMQ-1 exhibits the largest pore size ever reported among all existing stable zeolites (Supplementary Table 1). It has the second lowest framework density (11.4 Si atoms nm^{-3}) among all fully connected silicate zeolites and a very low density (1.14 g cm^{-3}). This is comparable with the 20-ring ZEO-5 zeolite (11.1 Si atoms nm^{-3}) obtained by a post-synthetic expansion of a complex chain silica zeolite precursor[22]. The presence of the extra-large 28-ring channels is also confirmed by annular dark field (ADF)-scanning transmission electron microscopy (STEM) images (Fig. 1c). The simulated PXRD pattern from the structure of calcined ZMQ-1 agrees well with the experimental PXRD pattern, further confirming the structure obtained from the cRED data (Extended Data Fig. 5b).

The dimensions of the extra-large pore in ZMQ-1 are extraordinary, yet its structural features bear similarities to common zeolite structures. The structure is built from wavy layers perpendicular to the *b* axis (in green), which are connected by flat strips extending along the *c* axis (in purple), as shown in Extended Data Fig. 6a–c. The strip contains 10-rings built of butterfly units commonly found in zeolites[27] (Extended Data Fig. 6c). A unique feature in ZMQ-1 is that all TO_4 tetrahedra in the butterfly net point in the same direction and connect to another butterfly net to form a double strip (Extended Data Fig. 6a,b). This differs from other zeolites built from butterfly units, in which different TO_4 tetrahedra in a butterfly net point in different directions[22]. The structure of ZMQ-1 contains typical composite building units of zeolites, *d5r*, *d6r* and *non*.

To understand the role of the OSDAs in the formation of the extraordinary channels in ZMQ-1, it is crucial to determine the position of the OSDA molecules in the structure. Therefore, we also investigated the as-synthesized ZMQ-1 by cRED (Extended Data Fig. 4d–f). cRED data of the as-synthesized ZMQ-1 collected at room temperature show that the crystals are monoclinic with the space group $P2/m$ and unit-cell parameters of $a = 18.94(3)$ Å, $b = 20.21(4)$ Å, $c = 27.51(7)$ Å and $\beta = 103.56(19)°$. The framework structure was determined on the basis of cRED data merged from three different crystals to achieve high data completeness. Similar to the calcined material, the as-synthesized ZMQ-1 also has extra-large 28-ring channels that are interconnected by 10-ring windows (Fig. 1e and Extended Data Fig. 6d). The main difference is that the 28-ring channels are tilted and bilobal shaped. This is confirmed by integrated differential phase contrast (iDPC)-STEM images (Fig. 1f). Local positional disorder was found for two symmetry-independent SiO_4 tetrahedra during the structure refinement, which were modelled using two different parts (Si29,30, O62–66 for PART 1 and Si31,32 and O67–70 for PART 2) with 56% and 44% occupancy, respectively. The tetrahedra associated to Si30 and Si32 have terminal groups at O66 and O70, respectively. Another terminal group is at O58, bonded to Si27. ADF-STEM images of as-synthesized and calcined ZMQ-1 show that the crystals are well ordered and free of defects (Extended Data Fig. 7a,b). The locations of symmetry-independent OSDAs were determined and refined using the low-dose cRED data (see Methods for detailed technical procedures). The final refined unit-cell compositions of calcined ZMQ-1 and as-synthesized ZMQ-1 are $[Si_{240}O_{480}]$ and $|C_{44}H_{82}P_2|_{2.65}[Si_{120}O_{240}(OH)_4]$, respectively. The number of OSDAs per unit cell is close to that obtained by elemental analysis (Supplementary Table 4). The PXRD pattern simulated on the basis of the structure of as-synthesized ZMQ-1 closely matches the experimental PXRD pattern, confirming the structure with OSDAs obtained from the cRED data (Extended Data Fig. 5c).

Notably, the octamethylene chain in each OSDA is interlocked by 10-ring windows. The tricyclohexylphosphonium heads extend into two different 28-ring channels. Because of their flexibility, the tricyclohexyl groups could not be located from the Fourier maps and they were instead added to complete the OSDA using Materials Studio (Fig. 1e and Extended Data Fig. 6d). The tricyclohexylphosphonium heads fill up the space of the extra-large 28-ring channel, which we believe plays an important role in directing the formation of the 3D framework and the intrinsic microporous and mesoporous 28 × 10 × 10-ring channel system. There are two symmetry-independent terminal hydroxyl groups (associated to O58 and O66/O70) in the as-synthesized ZMQ-1. Following calcination, the terminal hydroxyl groups condense and a fully connected framework is formed without any observed disorder (Fig. 1d,e and Supplementary Fig. 3). This results in the transformation of the bilobal-shaped channels into elliptical channels (Fig. 1d).

Physicochemical properties of ZMQ-1

It is well known that residual phosphorus remains within the micropores following calcination of zeolites obtained using phosphonium-based OSDAs. However, this residual phosphorus can be completely removed by washing with an ammonium chloride solution, as demonstrated in our previous work on extra-large-pore zeolites[28]. This removal is crucial as it allows for the evaluation of the true micropore volume without any blocking effect being caused by the residual phosphorus species. The Ar at 87 K physisorption of the ZMQ-1 zeolite after calcination and washing with NH_4Cl solution exhibits a type I(b) isotherm

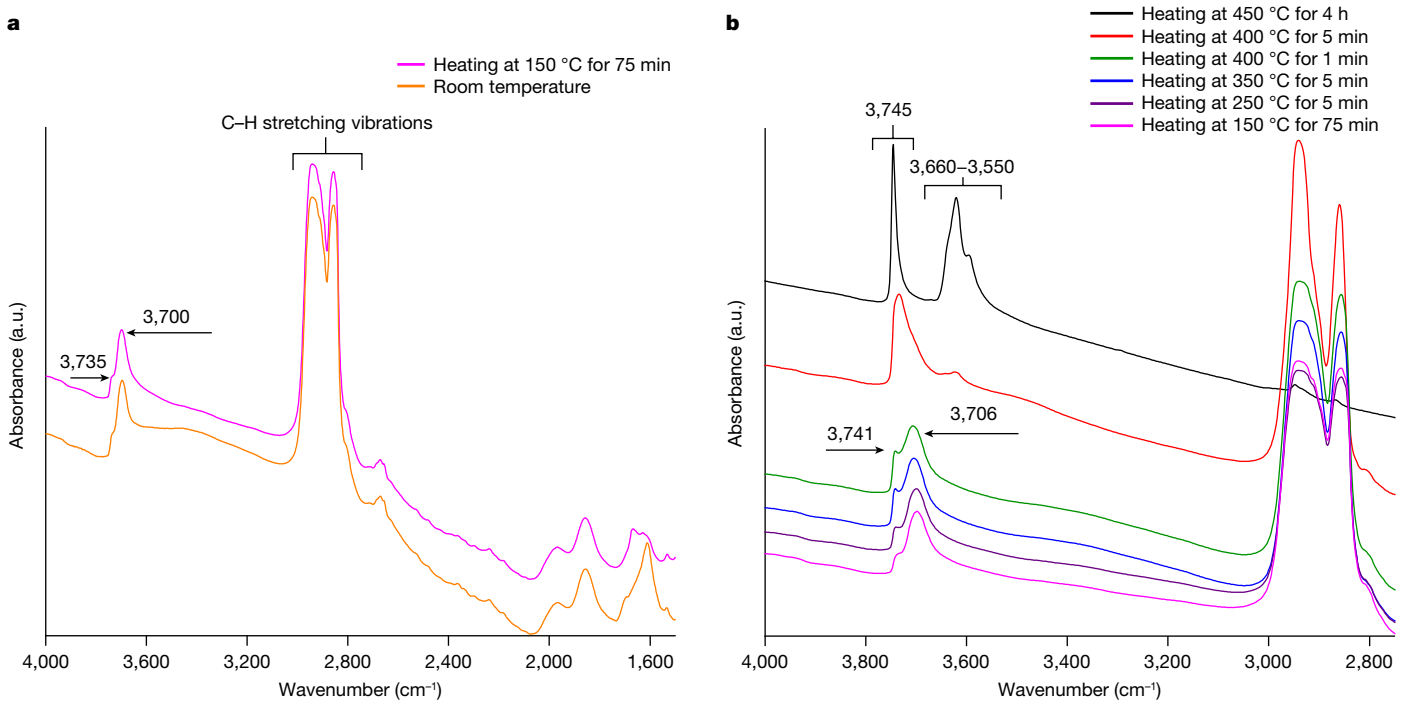

Fig. 3 | Temperature-evolved calcination of an as-synthesized ZMQ-1 through in situ FTIR. a, The infrared spectra for an as-synthesized ZMQ-1 before and after evacuation of water guest molecules at 150 °C. **b**, The series of infrared spectra collected after heating an as-synthesized pellet of ZMQ-1 under a dynamic vacuum of 10^{-6} torr. a.u., arbitrary units.

(Fig. 2b), consistent with the presence of extra-large micropores or narrow mesopores (<2.5 nm)[10]. The corresponding cumulative pore volume plot and pore size distribution were calculated using state-of-the-art nonlocal density functional theory (NLDFT) methods, considering a cylindrical pore model and a zeolitic surface (Fig. 2c). The data revealed two main volume uptakes associated with different pore sizes: one monomodal distribution centred around 0.5 nm and a more complex bimodal one with mode peaks centred at around 2.05 nm and 1.10 nm. The lower value (0.5 nm) can be naturally ascribed to a medium-pore-sized zeolite, consistent with the size of the 10MR channel (Fig. 2a). In the same way, the prominent peak centred at 2.05 nm fits well with the largest opening dimension of the 28MR and is close to the crystallographic mesopore size (2.28 nm). The other embedded peak located at 1.10 nm could originate from the smallest dimension of the 28MR (1.18 nm). The exact assignment of this intermediate volume to a specific network feature is not straightforward. Indeed, it should be stated that the NLDFT model used to calculate the pore size distribution only considers independent cylinders with molecularly smooth walls as a pore model. The apparent Brunauer–Emmett–Teller surface area of ZMQ-1 zeolites calculated from Ar adsorption data and using the Rouquerol criteria is about 1,447 $m^2 g^{-1}$, with a record-high zeolite pore volume of about 0.47 $cm^3 g^{-1}$ (Supplementary Table 4). The term 'zeolite pore volume' is proposed here to supplement the classical term 'micropore volume', as the mode pore size distribution of the material falls within the arbitrary limit set by the International Union of Pure and Applied Chemistry (IUPAC) to define the micropore and mesopore regions. Therefore, discussing an intraframework zeolite volume rather than micropore and mesopore volumes seems more logical. The as-synthesized and phosphorus-containing ZMQ-1 zeolites show high thermal and hydrothermal stability up to 800 °C (Extended Data Fig. 8c,d). Notably, the phosphorus-free ZMQ-1, after ammonium exchange, exhibits thermal stability comparable with the directly calcined phosphorus-containing ZMQ-1, maintaining stability even up to 1,000 °C (Extended Data Fig. 8e). Furthermore, phosphorus-free ZMQ-1 shows excellent hydrothermal stability up to 800 °C (Extended Data Fig. 8f) in a 50% relative humidity medium, comparable with its phosphorus-containing counterpart.

The ^{29}Si magic angle spinning (MAS) nuclear magnetic resonance (NMR) spectrum of the as-synthesized ZMQ-1 zeolite exhibits a wide peak ranging from −120 to −90 ppm. This corresponds to Q^4 and Q^3 species (Extended Data Fig. 9a), evidencing the structural disorder revealed by the structure refined against cRED data (Fig. 1d–f). Those defective sites condensed to become fully connected on thermal treatment starting at 400 °C, as observed during the temperature-evolved calcination of an as-synthesized ZMQ-1 through in situ Fourier-transform infrared spectroscopy (FTIR). Figure 3a shows the spectra collected under dynamic vacuum (10^{-6} torr) at room temperature and after heating at 150 °C for 75 min. The two bands between 3,000 and 2,800 cm^{-1} correspond to the C–H stretching vibrational band of the di-phosphonium OSDA. On heating at 150 °C, the broad band spanning between 3,600 and 3,000 cm^{-1} (corresponding to hydrogen-bonded hydroxyl groups and H_2O) and a sharp band at around 1,610 cm^{-1} (corresponding to the scissor bending vibrational band of H_2O) vanish, indicating the evacuation of residual water molecules. Furthermore, a band with a well-resolved maximum at 3,700 cm^{-1} and an overlapping sideband at 3,735 cm^{-1} are observed in the hydroxyl group stretching vibration region. On the basis of the literature findings[29–32], such bands are attributed to isolated and weakly hydrogen-bonded hydroxyl groups. This finding agrees with the figures describing the location of these species within the porous surface of ZMQ-1. The existence of two different vibrational bands for these silanol species is a result of their involvement in different hydrogen-bonding interactions within the ZMQ-1 framework. Figure 3b shows the spectra recorded under dynamic vacuum (10^{-6} torr) after heating the as-synthesized ZMQ-1 up to 450 °C. As the heating temperature reaches 400 °C for 1 min, both silanol bands are maintained and undergo a blueshift of 6 cm^{-1}, leaving the band at 3,741 cm^{-1} with a well-resolved maximum, yet remaining overlapped. Notably, on heating for an extra 4 min at 400 °C (total of 5 min), both silanol bands merge into a single band centred at 3,734 cm^{-1} with a broad half-bandwidth, accompanied by the appearance of a weak

band at 3,620 cm^{-1}, characteristic of Brønsted acid sites. After heating ZMQ-1 for 4 h at 450 °C, a sharp, well-resolved band also appears at 3,745 cm^{-1}, attributed to isolated hydroxyl groups. This observation suggests that the silanol species within ZMQ-1 undergo condensation along with the calcination of the OSDA, which leads to the healing of the defects observed with cRED. Mainly isolated silanol species remain after calcination. This is further supported by the ^{29}Si NMR of ZMQ-1 calcined-washed with NH_4Cl, for which sharper peaks above −106 ppm may be identified (Extended Data Fig. 9a), indicating a transformation in the hydroxyl groups following calcination. The complex multicomponent band between 3,660 and 3,550 cm^{-1} mainly corresponds to Brønsted acid sites formed after the removal of the OSDA, for which it is possible to distinguish a well-resolved maximum at 3,620 cm^{-1} with a weak shoulder at 3,635 cm^{-1} and a medium-intensity overlapping band at 3,595 cm^{-1}. This aspect of the Brønsted acid sites band might suggest that these sites are perturbed within ZMQ-1 owing to hydrogen bonding with neighbouring oxygen atoms.

In the as-synthesized zeolite, one main ^{27}Al environment is observed at 53.8 ppm, which corresponds to tetrahedrally coordinated sites in the zeolite framework (Extended Data Fig. 9b). After calcination, the zeolite shows two ^{27}Al broad environments at about 56.4 and −10 ppm. The former corresponds to Al in the tetrahedral sites. By contrast, the latter corresponds to different Al–O–P species[33], noting that a broad peak appears between 0 and −40 ppm in the ^{31}P NMR spectrum after calcination (Extended Data Fig. 1c). When the calcined zeolite is washed with ammonium chloride and then calcined again, tetrahedral ^{27}Al environments persist and a further sharp peak appears at 0 ppm assigned to extra-framework aluminium species (Al^{VI}). Besides, the phosphorus was not detected in the ^{31}P NMR spectrum (Extended Data Fig. 1c) and the ^{27}Al NMR peak at −10 ppm disappears as well (Extended Data Fig. 9b).

Catalytic properties of ZMQ-1

Since the adoption of zeolites by the petrochemical industry as an alternative to amorphous aluminosilicate catalysts, the quest to develop extra-large-pore zeolites has been primarily driven by the need to treat the heavy oil fraction of petroleum for economic value. This makes it of great interest to evaluate the catalytic performance of ZMQ-1 in vacuum gasoil (VGO) cracking as a benchmark test for its ability to valorize bulky molecules into value-added products. Here we tested ZMQ-1 zeolites after calcination (ZMQ-1(C)), which contains residual phosphorus species, and after subsequent washing with ammonium chloride (ZMQ-1(CW)) in the catalytic cracking of VGO and compared the results with commercial USY and Beta zeolites, as well as aluminium containing MCM-41 molecular sieve (see Methods for detailed experimental conditions and optimizations). Figure 4 shows that ZMQ-1 exhibits a comparable conversion rate of VGO to USY and Beta, and a much higher rate than MCM-41. In terms of product selectivity, phosphorus-free ZMQ-1 shows nearly the same selectivity as USY, with both materials favouring the formation of higher fractions of gasoline and diesel compared with Beta zeolite. Notably, phosphorus-containing ZMQ-1 shows a twofold higher selectivity towards diesel, accompanied by a twofold lower percentage of coke formation, which aligns with previous reports on phosphorus-containing extra-large-pore aluminosilicate ZEO-1. This brings the fuel selectivity (gasoline + diesel) for phosphorus-containing ZMQ-1 up to 80%, which is higher than its counterparts (see Extended Data Table 1). These preliminary catalytic test results highlight the strong potential of ZMQ-1 for acid-based heterogeneous catalysis, driven by its intrinsic mesoporosity and inherent phosphorus content, which does not require any post-synthetic treatment and competes well with USY zeolite, the horsepower of fluid catalytic cracking catalysis.

The characteristics of ZMQ-1 provide a new platform for fundamental research and diverse applications, including adsorption, separation, storage and ion exchange. Its intrinsic mesopores, robust framework and inherent acidity present new opportunities for advancements in process industries.

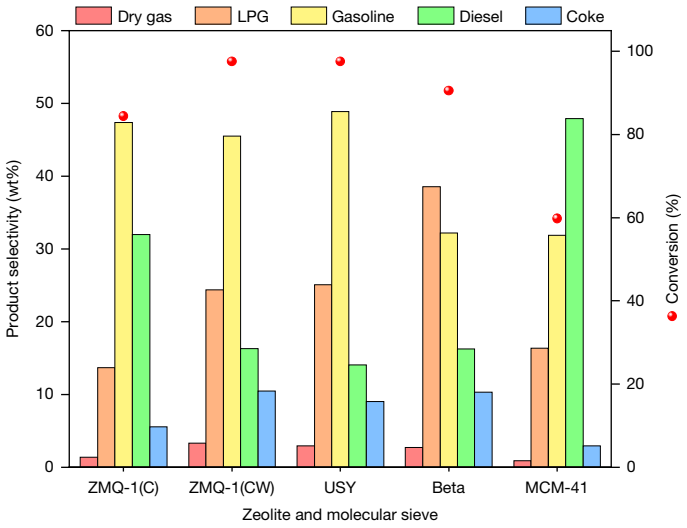

Fig. 4 | Catalytic performance of zeolite and molecular sieve catalysts. Catalytic cracking of VGO over ZMQ-1 and other catalysts. The Si/Al ratio of catalysts from left to right is 20 (ZMQ-1(C)), 28 (ZMQ-1(CW)), 15 (USY), 14 (Beta) and 15 (MCM-41). Reaction conditions: 500 °C, Cat/Oil = 0.59, 20–40 meshes (0.38–0.83 mm), 87 h^{-1} WHSV.

Online content

Any methods, additional references, Nature Portfolio reporting summaries, source data, extended data, supplementary information, acknowledgements, peer review information; details of author contributions and competing interests; and statements of data and code availability are available at https://doi.org/10.1038/s41586-024-08206-1.

1. Davis, M. E. Ordered porous materials for emerging applications. *Nature* **417**, 813–821 (2002).
2. Corma, A. Inorganic solid acids and their use in acid-catalyzed hydrocarbon reactions. *Chem. Rev.* **95**, 559–614 (1995).
3. Lu, P. et al. Few-unit-cell MFI zeolite synthesized using a simple di-quaternary ammonium structure-directing agent. *Angew. Chem. Int. Ed.* **60**, 19214–19221 (2021).
4. Dai, H. et al. Finned zeolite catalysts. *Nat. Mater.* **19**, 1074–1080 (2020).
5. Na, K. et al. Directing zeolite structures into hierarchically nanoporous architectures. *Science* **333**, 328–332 (2011).
6. Choi, M. et al. Stable single-unit-cell nanosheets of zeolite MFI as active and long-lived catalysts. *Nature* **461**, 246–249 (2009).
7. Zhang, X. et al. Synthesis of self-pillared zeolite nanosheets by repetitive branching. *Science* **336**, 1684–1687 (2012).
8. Han, S. et al. Cooperative surface passivation and hierarchical structuring of zeolite beta catalysts. *Angew. Chem. Int. Ed.* **61**, e202210434 (2022).
9. Serrano, D. P., Escola, J. M. & Pizarro, P. Synthesis strategies in the search for hierarchical zeolites. *Chem. Soc. Rev.* **42**, 4004–4035 (2013).
10. Thommes, M. et al. Physisorption of gases, with special reference to the evaluation of surface area and pore size distribution (IUPAC Technical Report). *Pure Appl. Chem.* **87**, 1051–1069 (2015).
11. Sing, K. S. W. Reporting physisorption data for gas/solid systems with special reference to the determination of surface area and porosity (Recommendations 1984). *Pure Appl. Chem.* **57**, 603–619 (1985).
12. Awala, H. et al. Template-free nanosized faujasite-type zeolites. *Nat. Mater.* **14**, 447–451 (2015).
13. Lee, H. et al. Synthesis of thermally stable SBT and SBS/SBT intergrowth zeolites. *Science* **373**, 104–107 (2021).
14. Li, X. et al. Machine learning-assisted crystal engineering of a zeolite. *Nat. Commun.* **14**, 3152 (2023).
15. Kresge, C. T., Leonowicz, M. E., Roth, W. J., Vartuli, J. C. & Beck, J. S. Ordered mesoporous molecular sieves synthesized by a liquid-crystal template mechanism. *Nature* **359**, 710–712 (1992).
16. Beck, J. S. et al. A new family of mesoporous molecular sieves prepared with liquid crystal templates. *J. Am. Chem. Soc.* **114**, 10834–10843 (1992).
17. Cassiers, K. et al. A detailed study of thermal, hydrothermal, and mechanical stabilities of a wide range of surfactant assembled mesoporous silicas. *Chem. Mater.* **14**, 2317–2324 (2002).
18. Sun, J. et al. The ITQ-37 mesoporous chiral zeolite. *Nature* **458**, 1154–1157 (2009).

19. Jiang, J. et al. Synthesis and structure determination of the hierarchical meso-microporous zeolite ITQ-43. *Science* **333**, 1131–1134 (2011).
20. Lin, Q.-F. et al. A stable aluminosilicate zeolite with intersecting three-dimensional extra-large pores. *Science* **374**, 1605–1608 (2021).
21. Li, J. et al. A 3D extra-large-pore zeolite enabled by 1D-to-3D topotactic condensation of a chain silicate. *Science* **379**, 283–287 (2023).
22. Gao, Z. R. et al. Interchain-expanded extra-large-pore zeolites. *Nature* **628**, 99–103 (2024).
23. Cichocka, M. O., Angstrom, J., Wang, B., Zou, X. & Smeets, S. High-throughput continuous rotation electron diffraction data acquisition via software automation. *J. Appl. Crystallogr.* **51**, 1652–1661 (2018).
24. Willhammar, T. et al. EMM-23: a stable high-silica multidimensional zeolite with extra-large trilobe-shaped channels. *J. Am. Chem. Soc.* **136**, 13570–13573 (2014).
25. Zi, W.-W. et al. An extra-large-pore pure silica zeolite with 16×8×8-membered ring pore channels synthesized using an aromatic organic directing agent. *Angew. Chem. Int. Ed.* **59**, 3948–3951 (2020).
26. Smeets, S. et al. Well-defined silanols in the structure of the calcined high-silica zeolite SSZ-70: new understanding of a successful catalytic material. *J. Am. Chem. Soc.* **139**, 16803–16812 (2017).
27. Guo, P., Wan, W., McCusker, L., Baerlocher, C. & Zou, X. On the relationship between unit cells and channel systems in high silica zeolites with the "butterfly" projection. *Z. Kristallogr. Cryst. Mater.* **230**, 301–309 (2015).
28. Fahda, M. et al. Investigating the physicochemical properties of an extra-large pore aluminosilicate ZEO-1. *Chem. Mater.* **36**, 5405–5421 (2024).
29. Zecchina, A. et al. Silicalite characterization. 2. IR spectroscopy of the interaction of carbon monoxide with internal and external hydroxyl groups. *J. Phys. Chem.* **96**, 4991–4997 (1992).
30. Bordiga, S. et al. Characterisation of defective silicalites. *Dalton Trans.* **21**, 3921–3929 (2000).
31. Bordiga, S. et al. Hydroxyls nests in defective silicalites and strained structures derived upon dehydroxylation: vibrational properties and theoretical modelling. *Top. Catal.* **15**, 43–52 (2001).
32. Dib, E., Costa, I. M., Vayssilov, G. N., Aleksandrov, H. A. & Mintova, S. Complex H-bonded silanol network in zeolites revealed by IR and NMR spectroscopy combined with DFT calculations. *J. Mater. Chem. A* **9**, 27347–27352 (2021).
33. Haouas, M., Taulelle, F. & Martineau, C. Recent advances in application of ^{27}Al NMR spectroscopy to materials science. *Prog. Nucl. Magn. Reson. Spectrosc.* **94–95**, 11–36 (2016).

Methods

OSDA synthesis

The OSDA used in this work is a di-quaternary phosphonium cation (bis-1,8(tricyclohexyl phosphonium) octamethylene, denoted as Tri-Cy-dC8, consisting of tricyclohexylphosphonium head groups connected by a linear methylene chain with eight carbons (Extended Data Fig. 1a). The synthesis of Tri-Cy-dC8 was carried out by the reaction of tricyclohexylphosphine with corresponding linear dibromoalkanes, $Br(CH_2)_8Br$. In a typical synthesis, 36.514 g (0.125 mol) of tricyclohexylphosphine (Aladin, >96%) was dissolved in 150 ml chloroform (Sinopharm, ≥99%) in a three-neck 500-ml flask immersed in an ice bath. The linear 1,8-dibromooctane (0.05 mol, Aladin, 98%) dissolved in 50 ml chloroform was added dropwise into the flask through an addition funnel. The mixture was stirred for 2 h and then heated to reflux for 4 days. After cooling to ambient temperature, excessive ethyl acetate was added to precipitate the white product, which was washed twice with ether and subjected to rotary evaporation to obtain the pure white OSDA dibromide salts. The structure and purity of the products were confirmed by liquid ^1H and ^{13}C NMR in D_2O (Supplementary Figs. 1 and 2).

The dibromide salts were converted to their corresponding hydroxide forms by anion exchange using anion exchange resin (Xidian, 1.1 mequiv/1 ml) in batch mode. The hydroxide solution was concentrated by rotary evaporation under vacuum. The concentration of the final solution was determined by titration with 0.1 N HCl (Beijing North Weiye Institute of Measuring and Testing Technology) using phenolphthalein as an indicator, and the weight percentage of the $OSDA(OH)_2$ is generally about 30 wt%.

Zeolite syntheses

Synthesis in the hydroxide medium. ZMQ-1 zeolite was initially discovered in hydroxide-mediated synthesis at 180 °C with a gel molar composition of $1.0SiO_2$:$0.02Al_2O_3$:0.25Tri-Cy-dC8$(OH)_2$:$10H_2O$. A typical synthesis procedure was as follows. 0.458 g (0.0022 mol) of aluminium isopropoxide (Macklin, AR) was dissolved in the $OSDA(OH)_2$ solution (0.0137 mol) in a plastic beaker under magnetic stirring, followed by 11.458 g (0.0549 mol) of tetraethyl orthosilicate (Sinopharm, ≥99%). The mixture was homogenized to obtain a clear sol, which was then hydrolysed at ambient temperature overnight to evaporate partial water and ethanol. The gel was then heated at 100 °C in a convection oven to remove residue water and ethanol to reach the target gel molar composition by weighting. The viscous gel was transferred into Teflon-lined autoclaves and heated at 180 °C in a convection oven statically for 10 days. The solid product was recovered by centrifugation and washing three times with water (200 ml), ethanol (100 ml) and acetone (100 ml), then dried at 100 °C for 12 h and subsequently calcined at 600 °C for 12 h with a ramping time of 6 h. The yield of the product is 98% based on SiO_2.

The crystallization time could be shortened to 5 days by increasing the crystallization temperature to 190 °C with the same gel composition following the procedure described above. Further, by varying the molar ratio of Al_2O_3, ZMQ-1 zeolites with different framework Si/Al ratios were successfully synthesized using the gel molar compositions of $1.0SiO_2$:$0.01Al_2O_3$:0.25Tri-Cy-dC8$(OH)_2$:$10H_2O$ and $1.0SiO_2$:$0.005Al_2O_3$:0.25 Tri-Cy-dC8$(OH)_2$:$10H_2O$. The solid product was recovered and processed according to the procedures described above.

ZMQ-1 was also successfully obtained by using fumed silica (Macklin, AR) and aluminium sulfate octadecahydrate (Sinopharm, AR) as Si and Al sources with different H_2O/SiO_2 ratios under static and rotation crystallization modes. In a typical synthesis, a synthesis gel with molar composition of $1.0SiO_2$:$0.02Al_2O_3$:0.25Tri-Cy-dC8$(OH)_2$:xH_2O, in which x = 10, 16 and 30, was prepared and then subjected to heating in Teflon-lined autoclaves in a static or rotation oven for different durations. The product was collected and processed according to the procedures described above.

Synthesis in the fluoride medium. ZMQ-1 zeolite was obtained from the fluoride medium with a gel molar composition of $1.0SiO_2$:$0.01Al_2O_3$:0.25Tri-Cy-dC8$(OH)_2$:0.5HF:$10H_2O$. In a typical procedure, aluminosilicate gel was first prepared according to that of the synthesis in hydroxide medium at 180 °C. Then, 0.596 g (0.0275 mol) of HF (48%) was added to the gel and the resulting mixture was homogenized for 10 min using a spatula. (Caution! This must be done in a fume hood because of the toxic and corrosive gases generated during the mixing process.) The obtained viscous gel was transferred into a Teflon-lined autoclave and heated at 190 °C in a convection oven statically for 10–15 days. The solid product was washed and then calcined according to the procedures mentioned above. The yield of product is 96% based on SiO_2.

Zeolite synthesis overview

The synthesis parameters and phases obtained are summarized in Supplementary Table 2. The first and foremost critical factor for the successful formation of ZMQ-1 phase is the introduction of Al, because pure silica syntheses in both hydroxide and fluoride media all produced unknown phase(s). Si/Al ratio in the synthetic gel ranging from 25 to 100 produced pure ZMQ-1 zeolites, but further increase and decrease of Si/Al directed to the unknown phase(s). Besides, heating temperature is vital for forming pure ZMQ-1 from aluminosilicate gel in hydroxide medium. Unknown phase(s) of little importance existed at a lower temperature of 180 °C, whereas they almost diminished at a higher temperature of 190 °C.

Removal of phosphorous species

Phosphorous species (oxides or phosphates) left in the calcined ZMQ-1 zeolites were removed by washing and ion exchanging with NH_4Cl solution. Typically, 0.2 g of calcined zeolite powder was mixed with 10 g NH_4Cl solution with a concentration of 1 mol l^{-1} in a sealed plastic bottle. The mixture was stirred in an oil bath at 80 °C overnight. The solid was collected by washing and filtration and then dried at 100 °C. The proton-form zeolite was obtained by calcining the above ammonium-form powder at 600 °C for 3 h with a 6-h ramp.

Thermal and hydrothermal stability test

The thermal stability of as-synthesized ZMQ-1 was tested in a muffle furnace at temperatures of 600 °C, 800 °C and 1,000 °C in air for 6 h, 1 h and 1 h, respectively, with a ramping rate of 6 h. The hydrothermal stability test was performed for the calcined zeolite (600 °C for 12 h) in a fixed-bed reactor at temperatures of 600 °C, 700 °C and 800 °C for 3 h with a relative humidity of 50% by purging deionized water with N_2 flow. 0.1 g of zeolite powder was placed in a quartz reactor tube supported by quartz wool and then heated under N_2 flow to the target temperature. Subsequently, deionized water was purged into the tube reactor by using a peristaltic pump to generate a mixture gas of N_2 and steam. After the 3-h treatment finished, the system was cooled to room temperature and the zeolite powder was taken out for analysis.

^{27}Al NMR shows that ZMQ-1 calcined at 600 °C and 800 °C have similar resonances centred at about 58.3, 41.9 and −9.7 ppm (Supplementary Fig. 4a), which could be assigned to Al species in tetrahedrally coordinated framework sites, distorted tetrahedrally coordinated framework sites and octahedrally coordinated framework sites interacting with polymeric phosphate species[34], respectively. By contrast, ZMQ-1 calcined at 1,000 °C shows the absence of resonance at about 58.3 ppm, indicating the possible disappearance of tetrahedrally coordinated framework Al. The prominent resonance at about 40.6 ppm is typically assigned to tetrahedrally coordinated Al in amorphous aluminophosphates formed by leached Al from the framework and P (ref. 35). Other resonances at 9.3 and −11.7 ppm could be assigned to octahedrally coordinated Al in aluminophosphates[36]. Ar adsorption–desorption isotherms and pore size distribution of the three calcined ZMQ-1 zeolites show that pore structure was preserved for zeolites

calcined at 600 °C and 800 °C but almost disappeared for the 1,000 °C counterpart (Supplementary Fig. 4b–d and Supplementary Table 5), indicating the collapse of the structure, most probably because of the dealumination as corroborated by ^{27}Al NMR spectra (Supplementary Fig. 4a). The thermal and hydrothermal stability of phosphorus-free ZMQ-1 (ZMQ-1(CW)) were also evaluated. ZMQ-1(CW) shows higher thermal stability up to 1,000 °C and hydrothermal stability comparable with that of phosphorus-containing counterpart (Extended Data Fig. 8e,f). The N_2 adsorption–desorption data of ZMQ-1(CW) calcined at different temperatures show decreased gas adsorption amounts and micropore volumes, along with elevated heating temperatures (Supplementary Fig. 5a and Supplementary Table 6).

General characterizations

Unless otherwise stated, the physicochemical characterizations have been performed for ZMQ-1 samples synthesized in hydroxide medium. Laboratory PXRD patterns of the zeolites were collected in a Rigaku LabView diffractometer (CuKα, λ = 1.5418 Å). High-temperature in situ PXRD was carried out on the same diffractometer with a Reactor-X cell, which has a Si sample holder in a heated chamber with a window made of Be foil. PXRD patterns of selected samples were taken during a heating programme at 5 °C min^{-1} heating rate at 50 °C steps up to 1,000 °C. At each step, the temperature was held for 1 min for PXRD recording. The morphology and size of zeolite crystals were examined using a Hitachi S-4800 scanning electron microscope equipped with a cold field-emission gun with an accelerating voltage of 2 kV. The technical details of the experimental set-up used for in situ FTIR analysis in this work have been described elsewhere[28]. Thermogravimetric analysis of the as-synthesized zeolites was performed using a Rigaku TG-DTA8122 thermal analyser system in 50 ml min^{-1} air flow with a heating rate of 10 °C min^{-1} from 30 to 1,000 °C. The textural properties of the zeolites after OSDA removal were investigated by physisorption of Ar at 87 K using a Micromeritics 3Flex instrument equipped with a cryostat I accessory. The samples were outgassed under vacuum at 350 °C for 12 h before measurement. Analysis parameters were carefully selected to ensure proper equilibration of the data. The apparent surface area was calculated using the Brunauer–Emmett–Teller method and following the procedure recommended in ref. 37. The cumulative pore volume and pore size distributions were calculated by applying the kernel of (metastable) NLDFT adsorption isotherms considering a zeolitic surface and isolated cylinders as a pore model. Although this model gives the best approximation available so far, validating the main mode pore sizes, it is evident that it does not perfectly describe the complex pore structure and potential surface roughness of the ZMQ-1 zeolite, that is, main elongated cylindrical-like pores interconnected by means of smaller cylindrical windows. Micropore volumes were also determined using the same kernel. The calculations were carried out using the VersaWin 1.0 software package provided by QuantaTec (Anton Paar). For comparison purposes, the zeolites were also analysed on a QuantaTec Autosorb iQ sorption analyser at 87 K. Statistically consistent results were obtained. Contents of Si, Al and P were analysed by inductively coupled plasma optical emission spectroscopy using an Elementar Unicube apparatus. We performed CHN analysis using a Thermo Fisher iCAP PRO analyser.

Solid-state NMR

^{29}Si, ^{27}Al and ^{31}P MAS NMR spectra were recorded on a Bruker Avance III HD 500 MHz spectrometer operating at 11.7 T using 4.0-mm rotors spun at ν_{MAS} = 14 kHz. The resonance frequencies of ^{29}Si, ^{27}Al and ^{31}P were 99.4, 130.4 and 202.6 MHz, respectively. For ^{29}Si MAS NMR, single-pulse duration of 2.33 µs corresponding to a flip angle of π/3 and a recycling delay of 20 s were used. 10,240 scans were acquired and chemical shifts were referenced towards teramethylsilane. For ^{27}Al MAS NMR, single-pulse duration of 1.75 µs corresponding to a flip angle of π/12 and a recycling delay of 1 s were used. 4,096 scans were acquired and chemical shifts were referenced towards aluminium nitrate ($Al(NO_3)_3$). For ^{31}P MAS NMR, single-pulse duration of 5.00 µs corresponding to a flip angle of π/2 and a recycling delay of 8 s were used. 1,600 scans were acquired and chemical shifts were referenced towards a saturated H_3PO_4 solution. ^{13}C cross-polarization magic angle spinning (CPMAS) NMR spectra were recorded on a Bruker Avance III 600 MHz spectrometer at a resonance frequency of 150.9 MHz. ^{13}C CPMAS NMR spectra were recorded using a 4-mm MAS probe and a spinning rate of 12 kHz. A contact time of 4 ms and a recycle delay of 2 s were used for the ^{13}C CPMAS NMR measurement. The chemical shifts of ^{13}C was referenced to teramethylsilane.

STEM

Samples for the STEM imaging were prepared by embedding a small amount (about 5 µg) of ZMQ-1 in LR White Resin within a gelatin capsule (size 00). The capsule was then hardened at 60 °C for 24 h. To create ultrathin sections with an estimated thickness of 50 nm, a Leica Ultracut UCT Ultramicrotome equipped with a 45° diamond knife from DiATOME was used. The sections were then transferred to Lacey carbon-supported copper grids. iDPC-STEM and ADF-STEM images of ZMQ-1 were obtained using a double aberration-corrected Themis Z TEM (Thermo Fisher Scientific) operated at an accelerating voltage of 300 kV. The images were acquired using a beam current of 10 pA, a convergence angle of 16 mrad and a dwell time of 5 µs. The iDPC-STEM images were formed using a segmented annular detector. A high-pass filter was applied to the iDPC-STEM images to reduce low-frequency contrast.

3D ED

Sample preparation. The as-synthesized or calcined ZMQ-1 samples obtained by means of the hydroxide route were dispersed in acetone and then the suspensions were treated by ultrasonication for about 30 s. One droplet from the suspension was applied on a Lacey carbon-supported copper TEM grid for further cRED data collection.

Data collection. cRED data were collected at room temperature on a JEOL JEM-2100 transmission electron microscope (LaB_6, 200 kV) using a high-speed Timepix hybrid camera (512 × 512 pixels, Amsterdam Scientific Instruments). The software Instamatic was used for the collection of cRED data. The crystals were rotated continuously at a rate of 0.45° s^{-1} during the data collection. The exposure time was 0.5 s per frame, which was integrated over 0.225° of reciprocal space. The electron flux density and camera length were 0.1 e$^-$ Å^{-2} s^{-1} and 25 cm, respectively.

To locate the OSDAs in the pores, low-dose cRED datasets were collected under cryogenic conditions on a 300-kV Titan Krios G2 equipped with a Ceta-D camera. The prepared TEM grids with the as-synthesized ZMQ-1 were plunge-frozen in liquid ethane and then transferred into the Krios through cryogenic transfer. To minimize the unnecessary electron exposure, EPU-D was used to ensure that the sample was exposed to the electron beam only during the data collection. A flux density of 0.0025 e$^-$ Å^{-2} s^{-1} was used, which gave a cumulative fluence of 0.375 e$^-$ Å^{-2} per dataset with a goniometer rotation range of 60°.

Data processing and structure determination. Rotation electron diffraction processing software (REDp) was first used to process cRED datasets to determine the unit cell and space group[38]. With the obtained unit cell and space group, cRED datasets were further indexed using X-ray detector software (XDS) to extract the reflection information[39]. For calcined ZMQ-1, the structure was solved from a single dataset using SHELXT. For as-synthesized ZMQ-1, three room-temperature datasets were merged based on their cross-correlation to improve completeness and I/σ(I). With the merged data, the average structure of as-synthesized ZMQ-1 was solved using SHELXT. The obtained structural models for both calcined and as-synthesized ZMQ-1 were further refined by SHELXL using the ShelXle GUI. All framework atoms were

refined anisotropically. Soft restraints on bond distances and angles were applied in the refinement. Electron diffraction frames that show severe dynamical effects (that is, electron diffraction frames taken close to zone axes) were excluded during the data processing.

Treatment of positional disorder in structure refinement of as-synthesized ZMQ-1

During the structure refinement, positional disorder was found for two (Si29 and Si30) out of 30 symmetry-independent Si atoms. Two more Si peaks, assigned as Si31 and Si32, were located at a distance of 1.1 and 1.3 Å to Si29 and Si30, respectively. They were grouped together with the other framework atoms by applying a shared site occupancy with Si29 and Si30. Four oxygen atoms coordinated with these disordered Si atoms were found to be split into two positions each, as suggested by SHELXL during the refinement. The disordered oxygen atoms were divided into two groups, associated with either Si29 and Si30 (assigned as O63–66) or Si31 and Si32 (assigned as O67–70). The PART instruction was used to group the disordered atoms, designated as PART 1 for Si29,30 and O63–66 and PART 2 for Si31,32 and O67–70. The structure including the disordered parts and later with the OSDAs (see below) was refined using restraints on some Si–O bond lengths and bond angles. The occupancy of the two disordered parts was refined to be 56% for PART 1 and 44% for PART 2.

Location of the OSDAs by low-dose cryo-cRED

Although the cRED data collected at room temperature gave high resolution (0.80 Å), it was not possible to locate the OSDAs in the pores. Therefore we collected new cRED data under cryogenic conditions (90 K) using a 40 times lower electron flux density (0.0025 $e^- Å^{-2} s^{-1}$) to mitigate electron-induced damage to the organic molecules (Supplementary Table 3). The low-dose cRED datasets were first indexed in *P2/m* using the XDS software to extract integrated intensities. To improve completeness and redundancy, ten datasets were scaled and merged into a single reflection file using XSCALE. Owing to the low dose, the data resolution was reduced to 1.08 Å, based on the $CC_{1/2}$ value. To locate the atomic position of OSDAs, a difference electrostatic potential Fourier map was calculated using the high-resolution framework model of the as-synthesized ZMQ-1 with the positional disorder against the merged low-dose cRED dataset. Two symmetry-independent OSDAs could be located from the difference electrostatic potential map. The positions of the phosphonium cations and carbon atoms in the octamethylene chains could be located and refined using soft restraints. The occupancies of the OSDAs were also refined to be 1.00 for OSDA1 and 0.70(5) for OSDA2. The tricyclohexyl groups could not be located, presumably because of their flexibility.

Catalytic cracking of VGO

The ZMQ-1 samples used for catalytic tests were synthesized in hydroxide medium, USY and Beta were supplied by Zeolyst and UOP, respectively, and MCM-41 was purchased from Tianjin Yunli Chemical Company. The VGO was provided by Sinopec Qingdao Petrochemical Co., Ltd. and its composition and properties are listed in Supplementary Table 7. The catalytic test was carried out in a fixed-bed reactor at 500 °C. The aluminosilicate zeolite catalysts were pelletized, crushed and sieved to 0.18–0.25 mm (60–80 mesh), 0.25–0.38 mm (40–60 mesh) and 0.38–0.83 mm (20–40 mesh) to screen out the appropriate pellet size to mitigate the influence of diffusion limitations. The pellet size range 0.38–0.83 mm was then selected and used for the systematic tests based on the experiment results (Supplementary Tables 8 and 9). In a typical experiment, 1.0 g catalyst (20–40 mesh) was mixed with 4 g quartz sand (20–40 mesh) and loaded into a stainless/quartz reactor tube with a diameter of 20 mm. Before the test, the catalyst was treated at 500 °C in N_2 flow at 40 ml min^{-1} for 20 min; then, the temperature was adjusted to the corresponding reaction temperatures. 1.7 g of VGO was injected at a constant rate on the catalyst bed with nitrogen as the inert carrier gas at a flow rate of 50 ml min^{-1}. Gaseous products were collected in a sample bag. The liquid products (C_{5+}) were collected in an ice bath downstream, which was kept at around 0 °C. The spent catalyst was stripped by nitrogen gas for about 30 min to recover the entrapped hydrocarbons. The gas and liquid products collected after the reaction were analysed using gas chromatography. Gases were analysed using an Agilent 7890A equipped with a HP-PLOT Al_2O_3 KCl column connected to a flame ionization detector for analysing C_1–C_6 hydrocarbons and Porapak-Q with a 5A molecular sieve column connected to thermal conductivity detectors for analysing H_2, N_2, CO, CO_2, H_2S and O_2. Liquids were analysed using a Agilent 7890A equipped with DB-1 columns connected to a flame ionization detector for analysing gasoline, diesel and heavy oil components. After completing the VGO cracking performance test of the catalyst, the spent catalysts were regenerated at 650 °C under flowing air for calculating coke deposition and the regenerated catalysts were also applied for the next catalytic tests. The VGO conversion and product selectivity of dry gas (H_2, H_2S, CH_4, C_2H_4, C_2H_6), liquefied petroleum gas ($C_{3,4}$), gasoline (C_{5+}, boiling point <200 °C) and diesel (C_{12+}, boiling point is 200–365 °C) were defined as follows:

$$\text{Conversion (\%)} = (W_F - W_H)/W_F \times 100\%$$

$$\text{Dry gas selectivity (wt\%)} = W_1/(W_1 + W_2 + W_3 + W_4 + W_c) \times 100\%$$

$$\text{Liquefied petroleum gas selectivity (wt\%)} = W_2/(W_1 + W_2 + W_3 + W_4 + W_c) \times 100\%$$

$$\text{Gasoline selectivity (wt\%)} = W_3/(W_1 + W_2 + W_3 + W_4 + W_c) \times 100\%$$

$$\text{Diesel selectivity (wt\%)} = W_4/(W_1 + W_2 + W_3 + W_4 + W_c) \times 100\%$$

$$\text{Light olefin selectivity (wt\%)} = W_o/(W_1 + W_2 + W_3 + W_4 + W_c) \times 100\%$$

in which W_F is mass of feed injected (g), W_H is mass of heavy oil with a boiling point above 365 °C in product, which is treated as an unreacted heavy oil, W_1 is mass of materials of dry gas components, W_2 is mass of materials of liquefied petroleum gas components, W_3 is mass of gasoline components, W_4 is mass of diesel components, W_c is the mass of coke deposition and W_o is the mass of specific light olefin in all products excluding the heavy oil.

Notably, for each VGO cracking run, a full mass balance was obtained. If the material balance was less than 95% or greater than 105%, the test was repeated. On the basis of the proposed possible reactions and detailed components obtained from gas chromatography, the mass balance is calculated as follows:

$$\text{Mass balance} = (W_1 + W_2 + W_3 + W_4 + W_c + W_H)/W_F \times 100\%$$

We carried out the tests at different weight hour space velocities (WHSVs; Cat/Oil ratios) for both USY and ZMQ-1(CW), and the data are summarized in Supplementary Fig. 6a and Supplementary Table 10. Five WHSVs were tested, that is, 44, 87, 175, 350 and 874 h^{-1} (corresponding to Cat/Oil of 1.18, 0.59, 0.29, 0.15 and 0.06, respectively), by changing the loading amount of zeolites and keeping the feeding amount constant. With the decrease of the WHSV, the VGO conversion increases for both zeolites. For ZMQ-1(CW) and USY, a conversion of 98% was obtained at a WHSV of 87 h^{-1}, but further decrease of the WHSV to 44 h^{-1} resulted in no obvious change in the conversion. Using the WHSV of 87 h^{-1}, parallel experiments using the fresh ZMQ-1(CW) and USY were performed to eliminate the experimental errors (Supplementary Fig. 7 and Extended Data Table 1). The standard deviation values calculated for the heavy oil conversion rates and product selectivities from three runs are small, proving the high reliability and stability of the reaction system and analysis method we have used in this work. Then, using the WHSV of 87 h^{-1}, we performed the consecutive reaction and regeneration tests for ZMQ-1(CW) to study the change in activity and deactivation behaviour. The data are shown in Supplementary Fig. 6b and Supplementary Table 11. For the five consecutive runs, no obvious deactivation was detected and the product distribution is almost consistent. The used

catalyst was recovered and characterized. It shows that the crystallinity is decreased after reaction but the crystal structure is still retained (Supplementary Fig. 5).

We performed five consecutive reactions without regeneration, which could be considered as quasi-time-on-stream tests, over USY and ZMQ-1(CW) zeolites, to study the deactivation profiles of the catalysts (Supplementary Fig. 8a). Both zeolites show monotonously decreasing activities along with incremental running times, that is, conversion declines from 95% and 96% to 64% and 60% for USY and ZMQ-1(CW), respectively, from the first to fifth run. ZMQ-1(CW) shows slightly lower activity after the initial reaction. Because the coke content could not be analysed using the present method, we further carried out incremental feeding from one to five times for each run, followed by reaction and regeneration, to obtain accumulated coke amount. The coke profiles show that ZMQ-1(CW) has larger accumulated coke, along with incremental feeding and reaction (Supplementary Fig. 8b), over that of USY, indicating that its intrinsic structure might be inducive to the large molecules formation. Comparing with reported optimized USY, Beta and extra-large-pore zeolites at comparable VGO conversion, ZMQ-1 shows higher yield towards fuels, preferentially for diesel, over that of ITT and JZO zeolites (Supplementary Table 12). Moreover, similar propylene yield is detected in ZMQ-1 and ITT.

Data availability

The crystallographic information files (CIFs) for the structures of as-synthesized and calcined ZMQ-1 zeolites are archived at the Cambridge Crystallographic Data Center (https://www.ccdc.cam.ac.uk/) under reference numbers 2348667 (as-synthesized ZMQ-1) and 2348668 (calcined ZMQ-1).

34. Simancas, R. et al. Versatile phosphorus-structure-directing agent for direct preparation of novel metallosilicate zeolites with IFW-topology. *Microporous Mesoporous Mater.* **317**, 111005 (2021).
35. Costa, A. F., Cerqueira, H. S., Ferreira, J. M. M., Ruiz, N. M. S. & Menezes, S. M. C. BEA and MOR as additives for light olefins production. *Appl. Catal. A Gen.* **319**, 137–143 (2007).
36. Lischke, G. et al. Spectroscopic and physicochemical characterization of P-modified H-ZSM-5. *J. Catal.* **132**, 229–243 (1991).
37. Rouquerol, J., Llewellyn, P. & Rouquerol, F. in *Studies in Surface Science and Catalysis* Vol. 160 (eds Llewellyn, P. L., Rodriquez-Reinoso, F., Rouqerol, J. & Seaton, N.) 49–56 (Elsevier, 2007).
38. Wan, W., Sun, J., Su, J., Hovmöller, S. & Zou, X. Three-dimensional rotation electron diffraction: software RED for automated data collection and data processing. *J. Appl. Crystallogr.* **46**, 1863–1873 (2013).
39. Kabsch, W. XDS. *Acta Crystallogr. D* **66**, 125–132 (2010).

Acknowledgements The ZeoMat Group acknowledges the starting grant provided by Qingdao Institute of Bioenergy and Bioprocess Technology and the support provided by the Shandong Energy Institute (SEI S202107). V.V., S.M., P.L. and X.Y. acknowledge the collaboration in the Sino-French International Research Network 'Zeolites' framework. P.L. acknowledges the support by Qingdao New Energy Shandong Laboratory of International Cooperation Project (QNESL ICP 202305). This work was supported by the Swedish Research Council (VR; grant no. 2019-00815 to X.Z. and grant no. 2019-05465 to T.W.) and the Knut and Alice Wallenberg Foundation for an equipment grant. TEM and cRED characterizations were performed at the Electron Microscopy Center (EMC) at Stockholm University through ARTEMI, a national research infrastructure for electron microscopy and the low-dose cRED was performed at the Cryo-EM Swedish Infrastructure Unit at SciLifeLab, Solna, Sweden. Z.Q. acknowledges the support by the National Natural Science Foundation of China (22178389). Z.L. is grateful for the support by the National Natural Science Foundation of China (22302218). We thank M. Lozier (Laboratoire Catalyse et Spectrochimie) for the physisorption measurements.

Author contributions V.V. and P.L. conceived and supervised the project. X.Z. led the structure determination part of the project, including structure refinement, location of OSDAs and topology analysis of the zeolites. Y.S. performed the syntheses and characterizations of OSDAs and zeolites. J.X. conducted all 3D ED experimental work, data collection, analysis and structure determination. R.G.-N. performed the physisorption analysis. M.F. performed the in situ FTIR analysis. E.D. carried out the solid-state NMR analysis. Z.L., Z.Q. and B.W. performed the reaction of catalytic cracking of VGO. T.W. conducted STEM imaging, model building, topology analysis and prepared structure models in the figure. H.X. co-supervised J.X. with data processing. J.C. collected and analysed the low-dose cRED data of as-synthesized sample at SciLifeLab. X.Y., Q.L. and H.Y. optimized the syntheses and characterizations of selected samples. S.M. contributed to the discussion and analysis of data. V.V., X.Z., P.L., J.X. and M.F. wrote the manuscript. All authors contributed to the discussion and revisions of the paper.

Competing interests P.L., V.V., Y.S., X.Y. and Q.L. have filed a patent on ZMQ-1 zeolite affiliated with Qingdao Institute of Bioenergy and Bioprocess Technology (China patent application no. 2023106333337; PCT application no. PCT/CN2023/106253).

Additional information

Supplementary information The online version contains supplementary material available at https://doi.org/10.1038/s41586-024-08206-1.

Correspondence and requests for materials should be addressed to Peng Lu or Valentin Valtchev.

Peer review information *Nature* thanks the anonymous reviewers for their contribution to the peer review of this work.

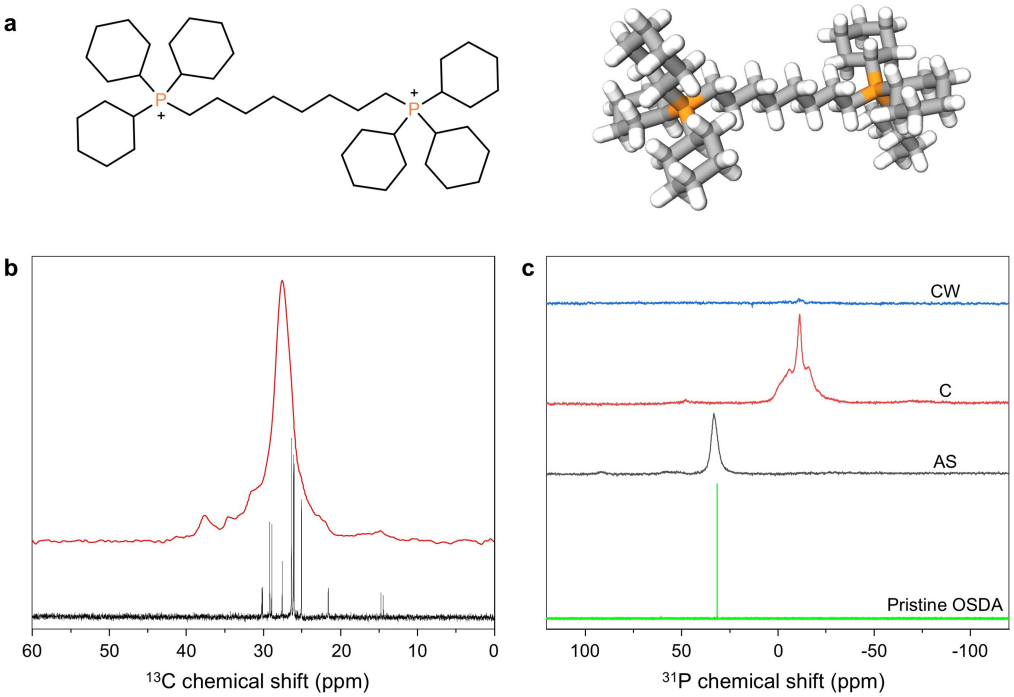

Extended Data Fig. 1 | The OSDA used in this work. a, The 2D (left) and 3D (right) structure of the OSDA. **b**, Solid-state ^{13}C MAS NMR of as-synthesized ZMQ-1 zeolite (red trace) and liquid-state ^{13}C NMR of pristine OSDA bromide (black trace) in D_2O. **c**, ^{31}P MAS NMR spectra of as-synthesized ZMQ-1 (AS), calcined ZMQ-1 (C), washed ZMQ-1 (CW) and liquid-state ^{31}P NMR spectrum of pristine OSDA bromide in D_2O.

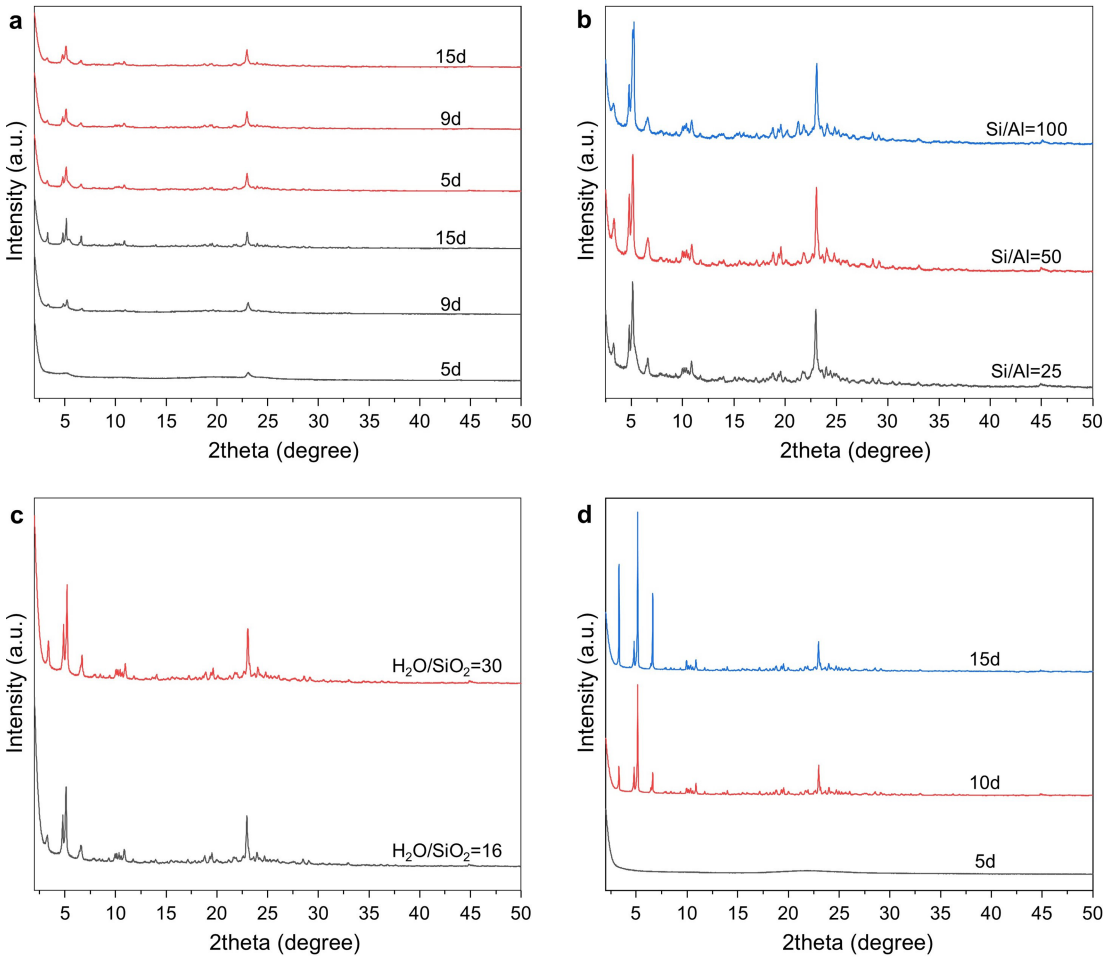

Extended Data Fig. 2 | PXRD patterns of zeolites obtained in various compositions and conditions. a, Zeolite obtained at 180 °C (grey traces) and 190 °C (red traces) from different crystallization times with a gel molar composition of $1.0SiO_2$:$0.02Al_2O_3$:0.25Tri-Cy-dC8$(OH)_2$:$10H_2O$. **b**, ZMQ-1 zeolites synthesized from gels with various Si/Al ratios using tetraethyl orthosilicate and Al(O*i*Pr)$_4$ as Si and Al sources in hydroxide medium at 190 °C. From bottom to top, the Si/Al ratios in as-synthesized product are 23, 35 and 68. **c**, ZMQ-1 zeolites obtained using fumed silica and $Al_2(SO_4)_3$·$18H_2O$ as Si and Al sources, with a gel Si/Al ratio of 25 at various H_2O/SiO_2 ratios, in hydroxide medium at 190 °C. **d**, ZMQ-1 zeolites obtained at different crystallization times in fluoride medium with a gel molar composition of $1.0SiO_2$:$0.01Al_2O_3$:0.25Tri-Cy-dC8$(OH)_2$:0.5HF:$10H_2O$ at 190 °C.

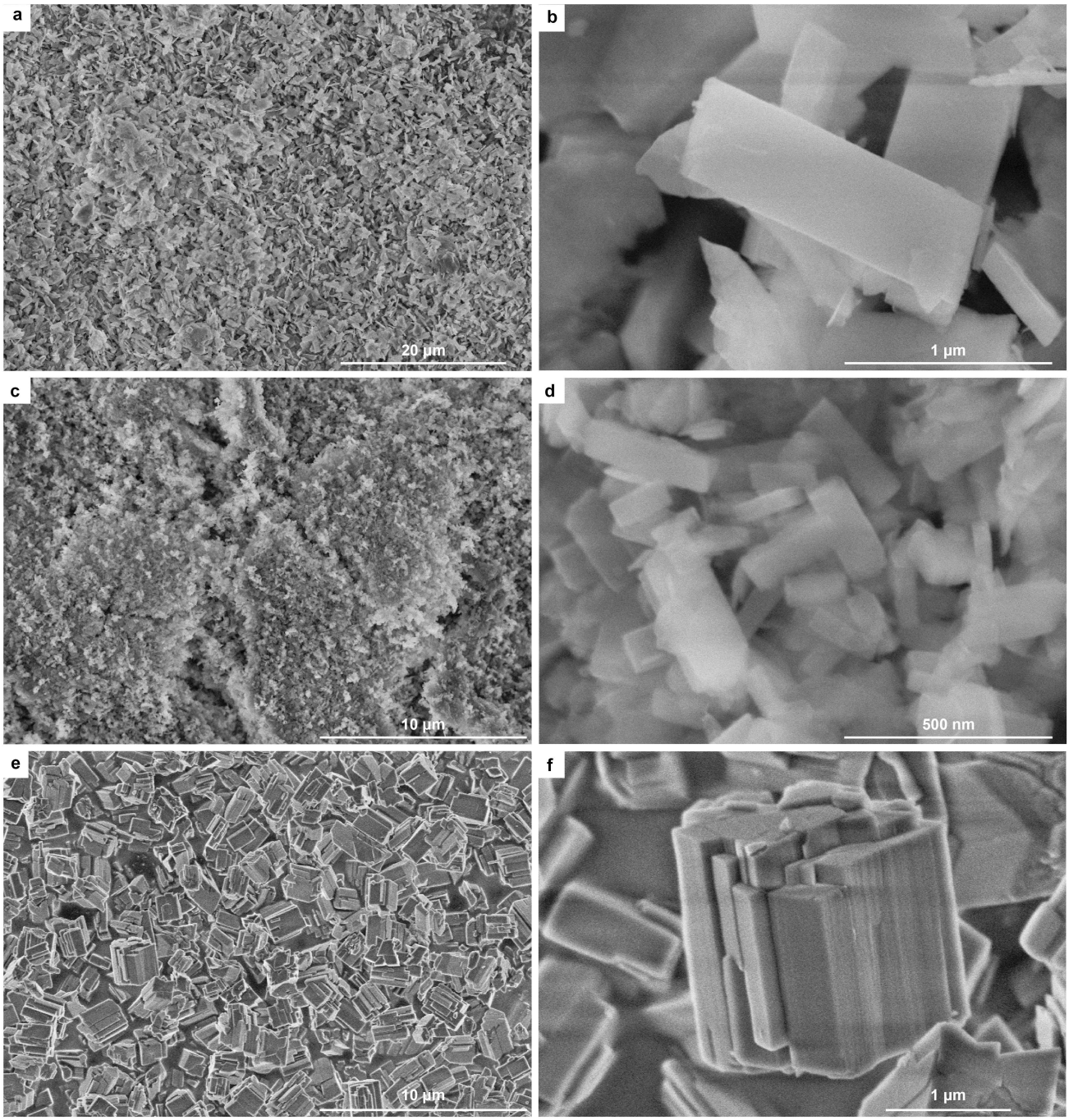

Extended Data Fig. 3 | Morphology of ZMQ-1 zeolites. Scanning electron microscopy images of ZMQ-1(OH) obtained at 180 °C (**a**,**b**), ZMQ-1(OH) obtained at 190 °C (**c**,**d**) and ZMQ-1(F) obtained at 190 °C (**e**,**f**).

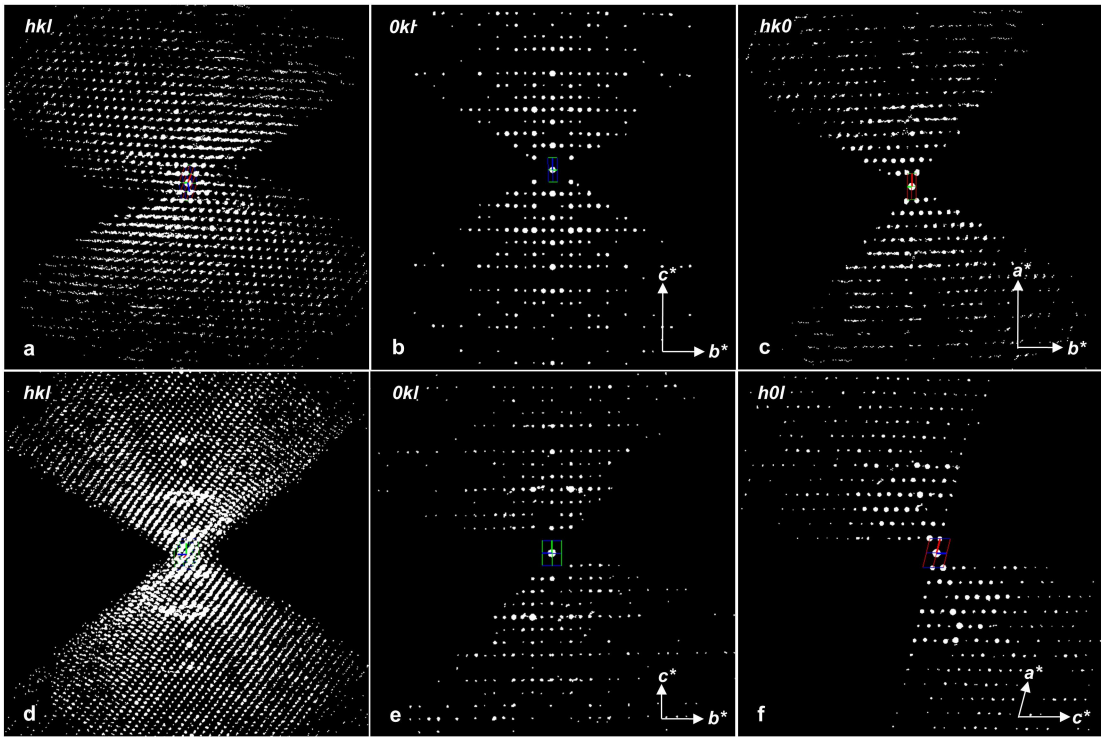

Extended Data Fig. 4 | cRED data from calcined ZMQ-1 and as-synthesized ZMQ-1. 3D reciprocal lattices reconstructed from typical cRED datasets of calcined ZMQ-1 (**a**–**c**) and as-synthesized ZMQ-1 (**d**–**f**). **a**,**d**, Projection of the 3D *hkl* reciprocal lattice. The corresponding 2D slices of reflections *Okl* (**b**) and *hkO* (**c**) cut from the calcined ZMQ-1 (**a**) and the corresponding 2D slices of reflections *Okl* (**e**) and *hOl* (**f**) cut from the as-synthesized ZMQ-1 (**d**).

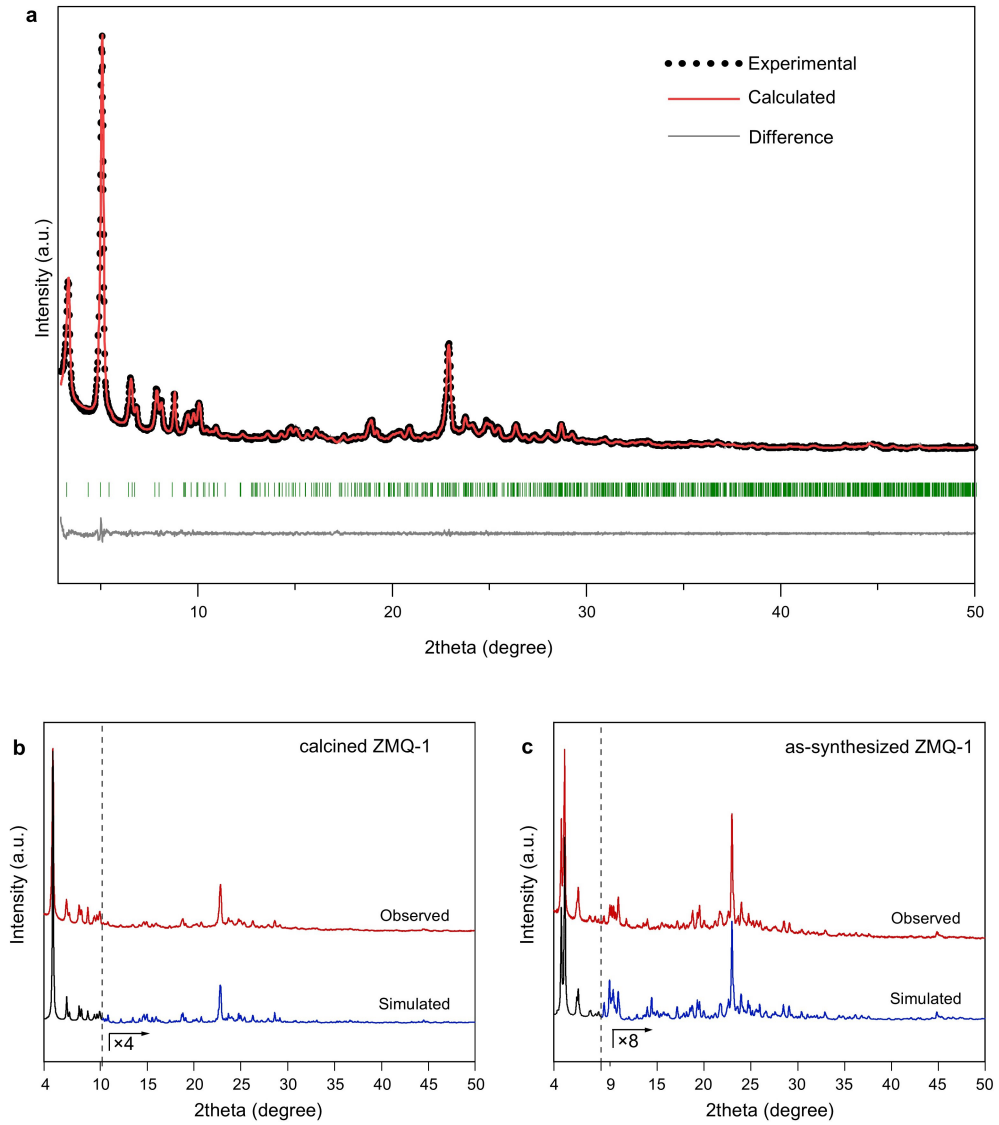

Extended Data Fig. 5 | Pawley fitting of calcined ZMQ-1 and comparison of simulated and observed PXRD patterns of ZMQ-1 (CuKα, λ = 1.5418 Å). **a**, The Pawley fitting against the in-house PXRD data (CuKα, λ = 1.5418 Å) was performed using the software Topas, which converged to R_{wp} = 3.51% and R_p = 2.64%, indicating the high purity of the sample. The peak positions are marked by green ticks. Simulated and observed PXRD patterns of calcined ZMQ-1 (**b**) and as-synthesized ZMQ-1 (**c**).

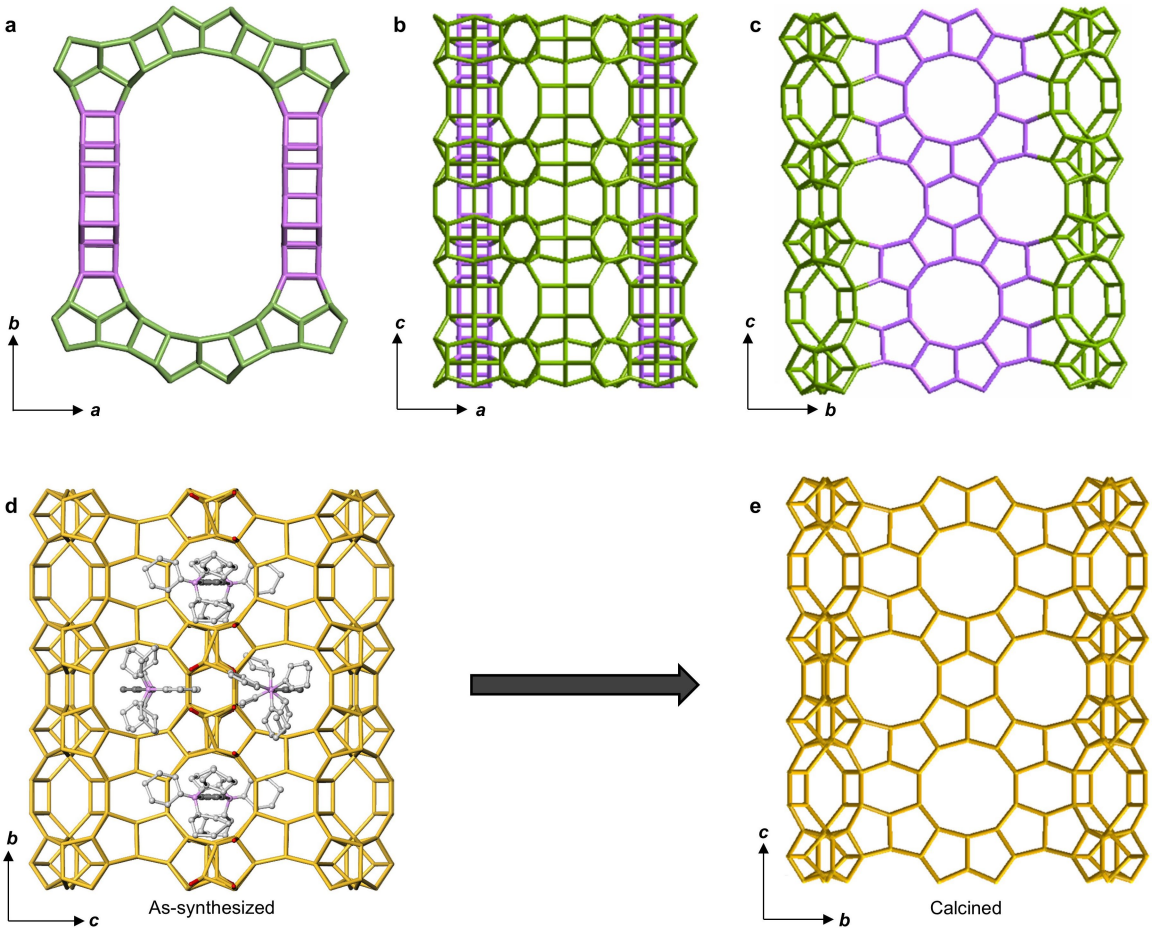

Extended Data Fig. 6 | Construction of the 28-ring channel of calcined ZMQ-1 and transformation of the ZMQ-1 structure by calcination. **a**–**c**, The 28-ring channel is constructed from a wavy layer (in green) and a double butterfly strip (in purple), as viewed along the *c* axis (**a**), *b* axis (**b**) and *a* axis (**c**). The structure of the as-synthesized (**d**) and calcined (**e**) ZMQ-1, viewed perpendicular to the extra-large 28-ring channel, showing the 3D 28 × 10 × 10-ring channel system. The locations of the OSDAs in the as-synthesized ZMQ-1 were determined from low-dose cryo-cRED data. The terminal hydroxyl groups condense to form a fully four-connected framework. Colour code: red, terminal oxygen; purple, phosphorus; dark grey, carbon determined by 3D ED data; light grey, carbon not located by 3D ED and added based on chemical information. Only the T···T connections of the framework are shown and H atoms are omitted for clarity.

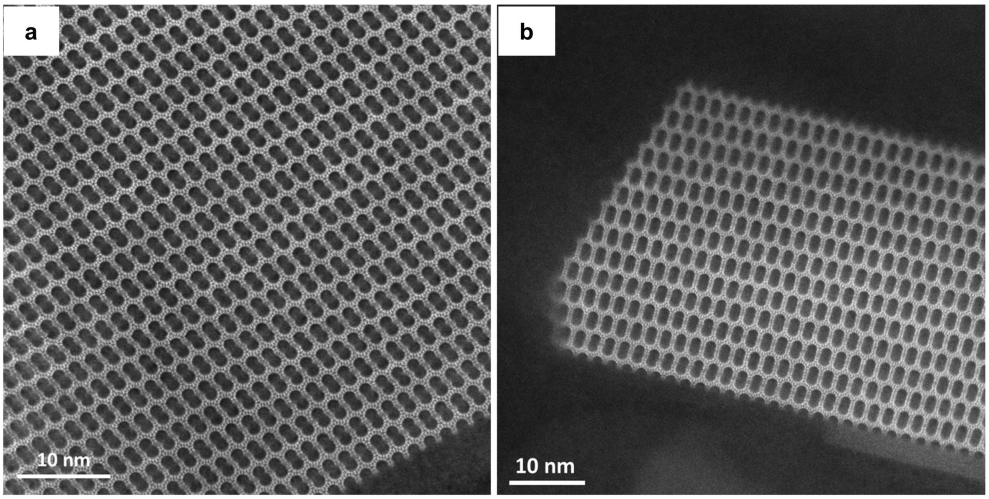

Extended Data Fig. 7 | ADF-STEM images of as-synthesized and calcined ZMQ-1 viewed along extra-large-pore channels. a, As-synthesized ZMQ-1 viewed along the *b* axis showing the extra-large bilobal-shaped channels. **b**, Calcined ZMQ-1 viewed along the *c* axis showing the extra-large channels.

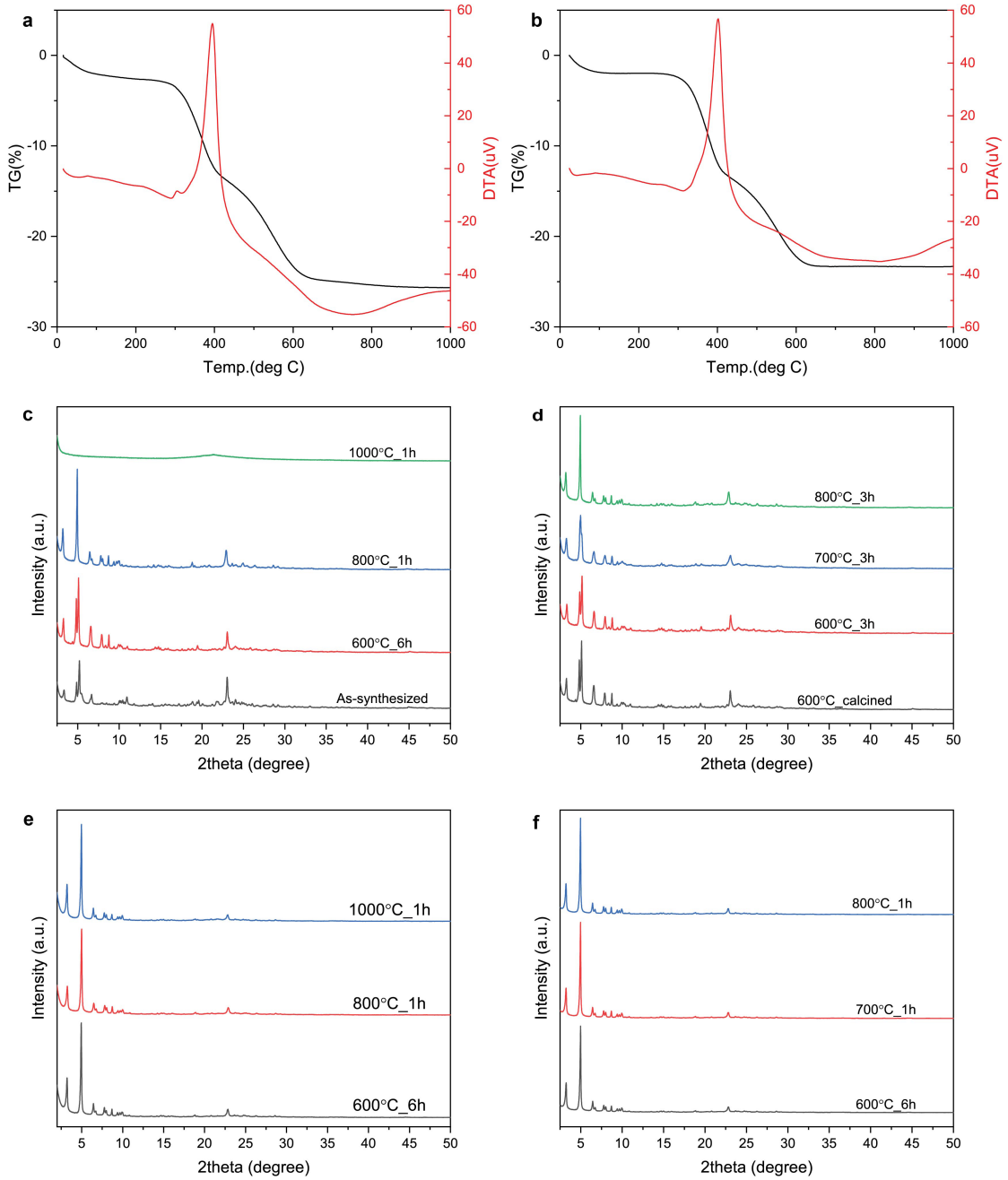

Extended Data Fig. 8 | Investigation of OSDA removal and thermal/hydrothermal stability testing of ZMQ-1 zeolites. a,**b**, TG and DTA analysis of as-synthesized ZMQ-1 obtained at 190 °C from hydroxide medium (**a**) and fluoride medium (**b**). **c**–**f**, PXRD patterns of various ZMQ-1 zeolites collected to evaluate thermal stability at different temperatures: as-synthesized ZMQ-1 (**c**) and calcined and NH_4Cl washed ZMQ-1 (**e**); and to evaluate hydrothermal stability at different temperatures under 50% relative humidity in water vapour. **d**, As-calcined ZMQ-1 containing residual phosphorus. **f**, Calcined and NH_4Cl washed ZMQ-1.

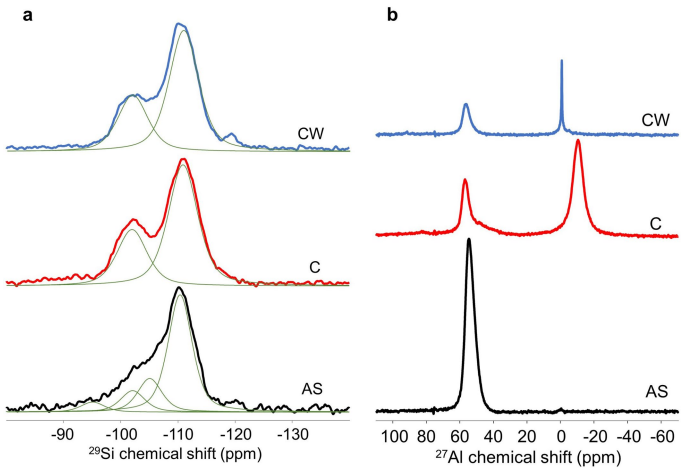

Extended Data Fig. 9 | Solid-state NMR analysis. a,**b**, ^{29}Si MAS NMR (**a**) and ^{27}Al MAS NMR (**b**) of as-synthesized (AS), calcined at 600 °C for 6 h (C) and calcined then washed with NH_4Cl then calcined at 600 °C for 3 h (CW) ZMQ-1 zeolites.

Extended Data Table 1 | Heavy oil conversion and product selectivity in catalytic cracking of VGO over proton-form zeolites at 500 °C

Zeolite	ZMQ-1(C) (20)[a]	ZMQ-1(CW) (28) [b]			Standard Deviation	USY (15)			Standard Deviation	Beta (14)	MCM-41 (15)
W_F[c]	1.7	1.7			-	1.7			-	1.7	1.7
W_H[d]	0.27	0.04	0.04	0.05	-	0.04	0.04	0.04	-	0.16	0.56
Conversion (%)	84	98	98	97	1	98	98	98	0	91	60
Selectivity (wt.%)											
Dry gas	1	3	3	3	0	3	3	3	0	3	1
LPG	14	24	25	24	1	24	26	25	1	39	16
Gasoline	47	46	45	46	1	50	49	48	1	32	32
Diesel	32	17	16	17	1	14	14	14	0	16	48
Coke	6	10	11	10	1	9	8	10	1	10	3
Fuel (Gasoline+Diesel)	79	63	61	63	-	64	63	62	-	48	67

[a]Si/Al ratios are given in parentheses following each zeolite. [b]On washing with NH_4Cl, a portion of the aluminium species (existing as extra-framework aluminium) is removed, which increases the Si/Al ratio from 20 to 28. [c]W_F is the mass of feed injected (g). [d]W_H is the mass of heavy oil with a boiling point above 365 °C in product, which is treated as unreacted heavy oil. Pellet size of zeolites is 0.38–0.83 mm (20–40 mesh). The Cat/Oil is 0.59 and the WHSV is 87 h^{-1}.